Boundary-Layer-Ingesting Inlet Flow Control

Lewis R. Owens*, Brian G. Allan† and Susan A. Gorton‡
NASA Langley Research Center, Hampton, VA 23681

An experimental study was conducted to provide the first demonstration of an active flow control system for a flush-mounted inlet with significant boundary-layer-ingestion in transonic flow conditions. The effectiveness of the flow control in reducing the circumferential distortion at the engine fan-face location was assessed using a 2.5%-scale model of a boundary-layer-ingesting offset diffusing inlet. The inlet was flush mounted to the tunnel wall and ingested a large boundary layer with a boundary-layer-to-inlet height ratio of 35%. Different jet distribution patterns and jet mass flow rates were used in the inlet to control distortion. A vane configuration was also tested. Finally a hybrid vane/jet configuration was tested leveraging strengths of both types of devices. Measurements were made of the onset boundary layer, the duct surface static pressures, and the mass flow rates through the duct and the flow control actuators. The distortion and pressure recovery were measured at the aerodynamic interface plane. The data show that control jets and vanes reduce circumferential distortion to acceptable levels. The point-design vane configuration produced higher distortion levels at off-design settings. The hybrid vane/jet flow control configuration reduced the off-design distortion levels to acceptable ones and used less than 0.5% of the inlet mass flow to supply the jets.

Nomenclature

A_C = inlet capture (highlight) area; area enclosed by inlet highlight (see fig. 3 for highlight definition) and tunnel wall, in.^{2}

A_0 = inlet mass-flow stream-tube at free-stream conditions, in.^{2}

* Research Engineer, Flow Physics and Control Branch, MS 170, NASA Langley Research Center, Hampton, VA 23681, Senior Member.
† Research Scientist, Flow Physics and Control Branch, MS 170, NASA Langley Research Center, Hampton, VA 23681, Senior Member.
‡ Principal Investigator, Subsonic Rotary Wing Project, NASA Langley Research Center, Hampton, VA 23681, Senior Member.

A_0/A_C = inlet mass-flow ratio, ratio of capture airflow to the ideal free-stream airflow, $\frac{A_0}{A_C} = \frac{\rho_C U_C}{\rho_0 U_0}$

c = VG vane chord length, in.

D_2 = duct diameter at AIP (see fig. 3), in.

$DPCP_{avg}$ = average SAE circumferential distortion descriptor (see equation 1)

$DPRP_i$ = SAE radial distortion descriptor for ring *i* on AIP total-pressure rake

h = height of vortex generator vane, in.

H = boundary-layer shape factor, δ^*/θ

H_i = height of inlet throat (see fig. 3), in.

M = free-stream Mach number

P/P_t = local AIP total pressure ratio to free-stream total pressure

P_t = free-stream total pressure, psi

$P_{t,2,avg}$ = area weighted average total pressure at AIP

$P_{t,2,avg}/P_t$ = inlet recovery pressure ratio

Rn/ft = Reynolds number per foot, 1/ft

Re_D = Reynolds number based on duct AIP diameter

T_t = free-stream total temperature, °R

U = velocity at each boundary-layer rake probe measurement, ft/sec

U_e = boundary-layer edge velocity, ft/sec

U/U_e = boundary-layer profile velocity ratio

W_{act} = airflow rate measured by venturi, lb_m/sec

α = VG vane angle to free-stream flow direction, degrees

δ = measured boundary-layer thickness, in.

δ^* = measured boundary-layer displacement thickness, in.

θ = measured boundary-layer momentum thickness, in.

Abbreviations:

AFC	active flow control
AIP	aerodynamic interface plane
BLI	boundary-layer ingesting
BWB	blended-wing-body
CFD	computational fluid dynamics
NASA	National Aeronautics and Space Administration
SAE	Society of Automotive Engineers
UEET	Ultra Efficient Engine Technology
VG	vortex generator

I. Introduction

In response to environmental concerns and to foster revolutionary propulsion technologies, NASA launched the Ultra Efficient Engine Technology (UEET) program in late 1999[1-3]. This program had several elements, one of which was to explore the feasibility of the Blended-Wing-Body (BWB) concept as an efficient alternative to conventional transport configurations. The BWB concept (Fig. 1) has been considered in various forms for several years[4-7]. Balance requirements for this configuration dictate the engine location on the aft section of the vehicle. The requirement to minimize the nose-down thrust moment places the engines closer to a waterline passing through the vehicle's center of gravity. However, this engine arrangement requires the incorporation of the inlets on the upper surface of the vehicle, which increases the technical risk of the configuration[6]. This risk includes the assumption that inlet flow control technology will be available to provide both uniform flow and adequate pressure recovery at each engine face when the inlet encounters significant boundary-layer ingestion (BLI).

The boundary layer on the aft portion of the BWB is estimated to be on the order of 30% of the engine inlet height, making the inlet design task a challenging one. A minimal level of inlet performance must be maintained throughout the flight envelope to provide enough uniform flow to ensure the engines continue to operate. The requirement for at least a minimum level of inlet performance under the severe conditions of an S-duct and a very large onset boundary layer flow have led to the consideration of using flow control devices in the inlet for this type

of application. Passive flow control in the form of vortex generating (VG) vanes can be used to improve the inlet flow[8-13]. Active flow control methods have also been investigated as a means to improve inlet flow for aggressive serpentine inlets with minimal BLI[12-13]. But the question still remains whether or not these devices can be applied effectively to manage the inlet flow with significant BLI in transonic flow conditions. The systems studies up to this point have assumed this to be the case.

In addition, the performance assessment of such a highly integrated propulsion system is a complex undertaking, requiring the simultaneous examination of many factors in order to determine whether BLI provides a benefit from an overall systems level viewpoint. The trade-offs among aircraft system parameters such as drag, weight, and engine performance must all be considered to assess the relative benefit of BLI inlet flow control technology. The effect of BLI on engine performance is known to be detrimental because BLI increases the distortion (flow non-uniformity) and reduces the pressure recovery at the engine fan-face[14]. Work done early in the development of the BWB configuration indicated BLI might improve the overall vehicle performance by as much as 10%[6]. NASA has continued to explore the benefits of BLI for the BWB, in a progressively higher fidelity manner. As part of the systems benefits assessment, NASA sponsored a contract with The Boeing Company in 2001 to assess the benefits of BLI inlets for a representative BWB configuration[15]. The predicted percentage flight range increase for flush-mounted BLI inlets compared to pylon-mounted inlets from this system study are shown in Figure 2. Additional system studies continue to point out the potential advantages of BLI inlets for the BWB configuration including less fuel burn and lower noise characteristics.

Researchers[15-28] are working to identify and develop active flow control devices and technologies for a variety of applications. This recent emphasis on active flow control and the progress in developing actuators, design tools, and control methodologies encouraged the hypothesis that a significant inlet boundary layer could be managed and improved by the application of active flow control. The current NASA study of BLI inlets has progressed through four phases to obtain the results presented in this report. Phase one included the development of a new high-Reynolds-number test capability for flush-mounted inlets in the NASA 0.3-meter Transonic Cryogenic Tunnel[29-31]. Phase two included the evaluation and selection of a control jet actuator system from simplified testing of control jets on an adverse pressure gradient ramp[28]. Phase three consisted of the low Mach number (M=0.15) testing of the selected control jet system with the BLI inlet geometry[15]. Finally, the fourth phase consisted of the high Mach

number (M=0.85) testing of the selected jet system with the BLI inlet geometry and is described in this report. A companion CFD study[32] guided the distribution of the control jets in the inlet during this phase of the investigation.

The purpose of the present investigation was to experimentally demonstrate inlet flow control with significant BLI at transonic Mach numbers and extend the inlet flow control experience beyond the previous low Mach number demonstration[15]. The present study was intended to answer the questions of whether or not the significant BLI could be managed at high Mach conditions and what mass flow requirements would be necessary to perform this task. The answer to both of these questions will affect future system studies dealing with BLI inlets. During an experiment in 2005, an S-shaped inlet with 35% BLI was tested at a free-stream Mach number of 0.85 over a range of the inlet mass flow settings. Flow control jets and vanes were used to provide flow control inside the inlet model. Measurements of inlet distortion and pressure recovery were made at a location corresponding to the engine fan-face, which is also referred to as the Aerodynamic Interface Plane (AIP), to provide a means to assess the flow control effectiveness.

II. Experimental Apparatus and Methods

A. Facility

The NASA Langley Research Center 0.3-meter Transonic Cryogenic Tunnel was used in this experiment[33-34]. The closed circuit, fan-driven tunnel has a 13 by 13-inch test cross-section with adaptive upper and lower walls. The facility can run in either an air or gaseous nitrogen mode of operation. The tunnel operates with total pressure ranging from 14.7 to 88 psia, Mach numbers ranging from 0.1 to 0.9, and Reynolds numbers up to 100 million per foot. A high-pressure air supply was used to supply the active flow control jets in the inlet model. The test could not be conducted at cryogenic temperatures because the air supply contained water vapor which posed the potential for frosting issues. The primary objective of this test was to examine the flow control effectiveness at high Mach number conditions, so high Reynolds number testing went beyond the scope of the study given the available resources. By using warm nitrogen gas, stable tunnel pressures could be achieved by balancing the vented mass flow by the inlet model with the injection of nitrogen into the tunnel.

B. Model

The model used in this experiment was designed and fabricated for the investigation by Berrier et al[31]. The inlet was designed in 2000 by Boeing to provide an inlet that was representative of a general class of inlets that could be

considered for application in a commercial BWB configuration. The definition of inlet parameters and a list of inlet characteristics are given in figure 3 and table 1, respectively. Pictures of the modified flush-mounted inlet on the tunnel sidewall are shown in figure 4. The 2.5%-scale inlet model is approximately 4.25 inches wide and 2.25 inches high with a one-inch tall boundary-layer rake on the side of the inlet, as shown in figure 4. The pressure difference between the tunnel total pressure and the atmospheric pressure drives the flow through the inlet. For this experiment, the ratio of the tunnel total pressure to the atmospheric pressure was approximately two.

The desired inlet flow operation range is summarized in table 2. The inlet mass flow ratio, A_0/A_C, operational range of interest is 0.46 to 0.65 at the cruise conditions of M=0.85 and a 36,000 feet altitude. The inlet model system used in the experiment could only produce A_0/A_C levels up to about 0.55 at the tunnel test conditions. This limited inlet mass flow ratio resulted from a problem of underestimating the displacement boundary layer thickness in the inlet design such that the inlet throat was not able to pass the higher mass flow rates[31].

C. Instrumentation and control jet system

The inlet instrumentation included surface pressure ports along the top, bottom and sidewalls of the diffuser. A total pressure (steady) rake with 40-probes was positioned at the AIP to measure pressure recovery and distortion. A portion of this rake is seen in figure 4a. The total pressure rake was designed to conform to the SAE standard[35]. Each rake arm is separated from the next by 45º. The frontal area for all eight-rake arms produced almost 15% blockage of the AIP area.

The tunnel 350-psig air system supplied the mass flow for the AFC jets. After passing through a mass flow meter, the control jet mass flow is split at a piping T-junction to supply two separate actuator manifolds. These actuators were compressed natural gas fuel injectors that acted as solenoid valves, which could be operated in either a steady or pulsed mode. In this test only the steady mode was used due to excessive tubing length and joint restrictions present in the test set up. Each actuator connected the manifold to the tubing that passed through the tunnel pressure shell and supplied air to the jet orifices in the inlet model. By changing the tubing arrangement, each actuator could be controlling two, four or six jet orifices in a variety of geometric patterns within the inlet. The number of control jets per actuator was always even because of the symmetry constraint imposed across the centerline of the diffuser. If one actuator was distributed to two control jets, then the jet mass flow rate was generally higher than if one actuator was connected to four or more control jets.

One of the control jet tubes was instrumented with a pressure transducer within six inches of the jet orifice. Similarly, another jet tube was instrumented with a thermocouple within about six inches of the jet orifice. The measurements were added to provide some guidance for setting jet boundary conditions for CFD simulations. Further analysis of this data is needed, but some general values for these measurements are included here for reference. The jet temperature was consistent for the entire test over all the test conditions covered. The jet temperature generally stayed about 70ºF, which was close to the measured air supply temperature. The jet pressure varied as the jet mass flow ratio increased. The maximum pressure level observed was about 75 psia at the maximum control jet mass flow rates. This jet pressure expanded into the inlet diffuser with measured static pressure levels around 25 psia for the tunnel total pressure test condition of 30 psia. This made the maximum jet pressure ratio tested approximately three.

An estimate of the uncertainty levels for key parameters is provided in table 3. These uncertainty estimates were developed using documented procedures[36].

D. Boundary Layer Assessment

Before studying the effects of BLI, assessment of the degree of BLI for the test setup was needed. The inlet model was scaled in the design process to achieve 30% BLI meaning the onset flow boundary layer height would be 30% of the inlet throat height. The inlet influences this oncoming boundary layer height, so it is not obvious where one should measure a varying quantity around the inlet model. One approach measures the boundary layer at the same tunnel station as the inlet lip highlight, but offset to one side of the inlet[31]. This approach was chosen for the present study so that relevant comparisons could be made with earlier research on the baseline inlet model. The boundary layer rake used in the present study is shown in figure 4. Measurements obtained during this test are shown in figure 5 along with a computed boundary-layer profile from the companion CFD study for this inlet model[37]. An inset view of the installed inlet model and boundary layer rake is included in the figure for reference. The analysis of these data suggested that the boundary layer height was insensitive to inlet mass-flow adjustments. The boundary layer height was approximately 0.6 inches and the profile shape compares fairly well with the computed one. In the detailed analysis of the boundary layer properties, the measured data produced five to six points in the fitted log region of the law of the wall plot. The law of the wall model with East's buffer region was used to integrate the boundary layer profile to the wall. The integration of the compressible boundary layer profile for the M=0.84 data gave a shape factor ($H=\delta^*/\theta$) of about 1.5, which is consistent with what is expected for a

compressible, turbulent, flat-plate boundary layer. Also, for reference the same boundary layer rake had been tested earlier in the empty test section at the location noted in the inset picture in figure 5. The empty test section rake measurement is in a different location, but provides another perspective to assess the boundary layer height on this tunnel wall. The inlet model test boundary layer profile measurements are similar to the empty test section boundary layer profile. Taking the ratio of boundary layer height of about 0.6 inches to the inlet model throat height of about 1.7 inches gives a value for the degree of BLI at about 35%.

The boundary layer rake was removed after the initial measurements were made for the test conditions covered in this test. The rake was removed because of the blockage effect that produced an asymmetric pressure distribution at the AIP. The rake blockage was significant enough to produce supersonic flow (calculated using local wall pressures) and the potential of shock interactions with the inlet flow field became a concern. The use of the adaptive tunnel walls did not sufficiently reduce the rake blockage. Figure 6 shows a comparison of the AIP rake pressure contours with and without the boundary layer rake installed. The boundary layer rake was on the side of the inlet that corresponded to the left side of the pressure contour plots shown in this figure. These pressure contours became more symmetric with the boundary layer rake removed. The rest of the test was performed without additional boundary layer measurements. The authors do not think the boundary-layer heights would change appreciably from those measured for the rake configuration even when the tunnel walls were changed to the symmetric wall settings used with the rake removed.

E. Adaptive Tunnel Walls

The inlet model scale (2.5%) was chosen to give a certain degree of BLI. This design approach produced a model that is large relative to the tunnel test section size, especially at transonic test conditions. The adaptive tunnel walls, which lay on either side of the inlet model, were used to reduce some of the expected wall interference. The adaptive wall positions used throughout the test are shown in figure 7. The delta wall positions plotted in the bottom of this figure show each wall displacement from a parallel wall position.

Figure 8 presents a typical local Mach number distribution with the wall shape used throughout the test. The flow enters the test section at M=0.88 and begins to slow down to about M=0.85 before reaching the inlet model location (based on pressure data measured on wall opposite of the inlet). After reaching the inlet, the flow accelerates slightly before dropping to a new Mach number level after the inlet. This Mach level drop after the inlet

(stations 15 to 25 inches) is caused by the tunnel mass flow removal by the inlet that cannot be replaced and appears to the flow as an effective cross-sectional area increase.

F. Flow Control Devices

Two types of flow control devices were used to manipulate the flow inside the inlet diffuser. The two devices were air jets and vortex generator vanes. The general layout of the two types of flow control devices is shown in figure 9. The view is of the left half of the inlet diffuser as seen from a downstream, three-quarters-view perspective. In the figure on the left, the available air control jet locations are generally shown. CFD simulations guided the selection of these jet locations[32]. There are a total of 176 control jet orifice locations distributed along 11 different axial stations. Each jet orifice had a diameter of 0.040 inches and was skewed 90º to the oncoming flow with a 30º upward pitch from the local surface tangent. Figure 10a shows the typical jet orientation at an inlet cross section to deflect the oncoming flow away from the bottom centerline. This approach was taken to counter the secondary inlet flow that is produced by the higher static pressure at the top of the diffuser than at the bottom, which tends to cause low momentum boundary layer flow to collect in the bottom of the diffuser. The jets were oriented to primarily impart momentum to produce a side force on the local flow and secondly to create vorticity.

The vortex generator (VG) vane configuration tested is shown on the right side of figure 9. The layout of these VGs was obtained from a design-of-experiments CFD analysis[38]. The VG design placed groups of six vanes in four different regions toward the front of the diffuser (see figure 10b). Two of these groups are shown in figure 10, one on the left bottom of inlet and the other on the left side of the inlet. The VG groups on the bottom of the inlet had a design height of 0.181 inches (h/D_2=0.074) and were angled 12.9° to the oncoming free stream flow. The VG groups on the sides of the inlet had a design height of 0.163 inches (h/D_2=0.065) and were angled 11.5° to the oncoming free stream flow.

III. Discussion of Results

A. Effects of control jets on inlet flow distortion and pressure recovery

The inlet distortion in this investigation was described by the SAE circumferential distortion descriptor, $DPCP_{avg}$, which is defined in the Aerospace Recommended Practice (ARP) 1420 standard[35]. The $DPCP_{avg}$ is equal to the average distortion intensity defined in (1).

$$DPCP_{avg} = 1/N_{rings} \sum_{(i=1-5)} Intensity_i \quad (1)$$

where i is the ring number on the AIP rake and N_{rings} is the total number of rings. The Intensity for each ring is defined as,

$$Intensity_i = (PAV_i - PAVLOW_i)/PAV_i \quad (2)$$

where PAV_i is the average total pressure of ring i and $PAVLOW_i$, the area average of the low total pressure region below PAV_i.

The effect of the control jets on the circumferential distortion is shown in figure 11. The control jet distribution used for this active flow control case is shown in the inset picture in the upper right-hand side of the figure for reference. The distortion is plotted versus the total control jets mass flow rate normalized by the inlet mass flow rate for this test condition. These distortion curves show an initial distortion plateau region that occurs from 0 to 0.75% control jet mass flow ratio. Above a control jet mass flow ratio of 0.75%, the distortion begins to decrease until reaching a minimum distortion level at a jet mass flow ratio of 2.6%. For most of the test, the tunnel total pressure level was set to 30 psia, which increased the available range of the ratio of jet pressure to the internal diffuser pressure (i.e., jet pressure ratio) making the jet control more effective. As shown in figure 11, the effect of tunnel total pressure variation was examined briefly. The doubling of the tunnel total pressure also doubled the Reynolds number. Over the Reynolds number range covered there did not appear to be any significant influence of the Reynolds number on the distortion levels. This result agrees with the findings from the baseline inlet Reynolds number investigation[31].

The circumferential distortion goal was determined by correlating distortion levels from various known experiences. Generally acceptable $DPCP_{avg}$ levels for commercial applications are stated to be below about 0.04 to 0.05[31]. Looking at another distortion descriptor, DC(60), the acceptable levels occur below 0.10 for civil and 0.20 for military applications[14]. Different inlet research studies base their results on different distortion descriptors. The authors of this study decided to use the distortion descriptor presented in the SAE standard[35]. To relate $DPCP_{avg}$ to a distortion goal, an approximate relationship between two distortion descriptors was assumed. From numerical studies[38] modeling the flow control application for the same BLI inlet geometry, it was observed that the $DPCP_{avg}$

values were about a tenth of the DC(60) values. Since the program target distortion level goal was set at or below a DC(60) level of 0.20, the corresponding $DPCP_{avg}$ level was set to 0.02 or lower.

Physical insights into these distortion data in figure 11 are gained by examining the total pressure contours from measurements at the AIP. These contours show four different distortion levels along these distortion curves. Starting at the far left, the pressure contour shown is typical for the baseline (no flow control) inlet flow field. The upper half of the AIP has high total pressure levels, which represents undistorted inlet flow. The bottom half of the AIP has low total pressure regions characteristic of low momentum boundary layer flow that moves toward the bottom of the inlet. This flow collects at the bottom of the inlet because of the secondary flow generated by the static pressure difference between the upper (high static pressure) and lower (low static pressure) surfaces of the forward part of the diffuser[14]. The plateau region in the distortion curve results from all the jet momentum going towards balancing the effect of this secondary flow. Up to a jet mass flow ratio of 0.75% there has been marginal progress in dealing with the BLI problem. The next pressure contour at the jet mass flow ratio of 1.0% was selected to demonstrate why the distortion level is starting to decrease. In this contour plot, the low total pressure region at the bottom of the diffuser has begun to be spread around the circumference of the AIP. At this point, the control jets have balanced the secondary flow forces and have only just begun to deal directly with the BLI problem. The next two total pressure contours show the effects of the increased jet momentum to continue to spread the boundary layer around the circumference of the diffuser, which continues to decrease the circumferential distortion level. The last total pressure contour begins to show signs of the boundary layer flow collecting on the sides of the AIP at the minimum distortion level attained. This collection of the low momentum flow on the sides of diffuser suggests the jet distribution is no longer adequate to effectively deal with the BLI problem. The bottom jets for this configuration have cleared too much of this flow from the bottom of the diffuser and there are also not enough side jets to help clear some of this flow from the sides toward the top of the AIP. Therefore the inefficiency of the jet distribution at this distortion level explains why the distortion level has hit a minimum here.

The pressure recovery trends that correspond to the distortion curves discussed above are presented in figure 12. In general, the pressure recovery decreases approximately 0.01 as the distortion level decreases. The starting pressure recovery level of 0.95 is lower than that of a non-BLI inlet application, which is about 0.98. Ingesting the oncoming boundary layer causes the lower pressure recovery for the baseline (no flow control) inlet. If one integrates total pressure in the boundary layer profile shown in figure 5 across the inlet capture area and ratios this to

the free-stream total pressure for the same area, the result is about 0.95. This shows the connection between the ingested boundary layer and the reduced pressure recovery level for the baseline inlet. The pressure recovery for the baseline inlet is lower than expected and adding inlet flow control produces a further decrease in the pressure recovery level. Normally, the baseline inlet of this type is expected to have internal lower surface separated flow regions that are reduced as flow control is added increasing the total pressure recovery. However, the baseline inlet in this case does not appear to have any significant flow separation regions. The unexpected decrease in the pressure recovery with flow control is probably associated with viscous flow interactions between the control jets and the oncoming flow causing a loss of energy as well as some contribution of pressure measurement error due to the high flow angularity the flow control can produce at the AIP. To reduce the viscous losses (flow separation), it may be necessary to change the jet orientation (i.e., skew jets to point more downstream). This jet orientation change needs to be balanced with an increased jet mass flow rate necessary to produce sufficient side force to deflect the oncoming flow to a similar degree. CFD results[37] predict a similar pressure recovery trend with jet mass flow rate increase. From these CFD results, the local flow angularity was determined at the AIP. For the flow control cases, the maximum local flow angles were as much as 30° and generally occurred toward the side regions (±90° from top center) of the duct flow. Applying a total pressure error correction to experimental pressure measurements in these regions accounted for about 0.002 of the 0.01 pressure recovery decrease. At this time, it is conjectured that the local flow separations near the flow control jets account for the majority of the decrease in pressure recovery with flow control.

The pressure recovery trends did indicate a small effect of increasing Reynolds number. In the regions of the pressure recovery curves where the data overlapped, the pressure recovery increases as the Reynolds number increases. This Reynolds number trend is consistent with that observed in the baseline inlet Reynolds number investigation[31]. The pressure recovery is generally expected to increase as flow deficits are reduced. Increasing the Reynolds number decreases the boundary layer thicknesses to produce this effect.

B. Effects of jet momentum and distribution on inlet flow distortion and pressure recovery

The impact of different control jet momentum and jet distributions on the effectiveness to reduce the circumferential inlet distortion is presented in figure 13. The number of jets and their placement are key to producing an effective inlet flow control approach. The diameter of the jet orifice also plays a major role. However, for the current study the jet orifice diameter remained constant. The distortion trends presented were selected to

represent some of the configurations tested that most effectively reduced the circumferential distortion. An inset picture of the jet distribution pattern is included for each of the distortion curves to give a sense of how the jet distribution correlates to the distortion reduction effectiveness. The jet patterns with the lowest number of jets tended to overcome the secondary flow and started reducing the distortion at lower control jet mass flow ratios than those with a higher number of control jets. This behavior appears to be related to the higher per jet momentum producing initially more effective distortion reduction configurations. However, comparing the two distortion curves for the two configurations with 16 jets shows the importance of the jet distribution pattern. One of these two configurations shifted the jet distribution from being concentrated near the diffuser bottom centerline to spreading the jets more toward the sides of the diffuser. In this comparison, the jet momentum for each jet would be similar such that the jet distribution is the primary driver in each pattern's distortion reduction effectiveness. The configurations which tended to show the largest reductions in the inlet distortion tended to have more jet orifices distributed along the sides of the diffuser. Referring back to the pressure contour for the minimum distortion level shown in figure 11, increasing the number of jets on the sides of the diffuser to keep the spreading boundary layer from collecting on the sides seems to be a necessary approach in dealing with the BLI inlet distortion problem. So, the most effective distortion reduction configurations are those that effectively balance both the control jet momentum as well as the distribution of those jets inside the inlet diffuser. Higher per jet momentum for jet orifices evenly distributed between the forward bottom and sides of the diffuser are potentially the best jet patterns to consider for this type of active flow control application. It is important to maximize the jet efficiency by selecting an optimal number of jets, producing the highest total jet momentum for a given jet mass flow rate, while also optimizing the spatial distribution of the selected jets.

The pressure recovery trends for the different control jet patterns with varying control jet mass flow ratios are shown in figure 14. The general trend of pressure recovery loss with increasing control jet mass flow rate is similar to that discussed in figure 12. However, the 30-jet configuration did show a little higher pressure recovery for jet mass flow ratios above 1.5%.

C. Effects of circumferential distortion reduction on radial distortion

Redistributing the ingested boundary layer around the circumference of the AIP causes the reduction of the circumferential distortion in the inlet. This redistribution of the low momentum flow reduces the gradients circumferentially but increases them in the radial direction. A radial distortion pattern representative of all the flow

control data acquired during the current test is shown in figure 15. Each symbol corresponds to a different circumferential inlet distortion level. The magnitude of the radial distortion consistently increased as the circumferential distortion levels decreased. In the flow control approach taken to deal with this type of BLI problem, the boundary layer is not removed. Instead, the boundary layer is shifted from one gradient pattern to another. The circumferential distortion level is the most important constraint to meet when compared to radial distortion. There will always be some level of radial distortion caused by viscous effects on the inlet duct walls. This approach to inlet flow control for BLI inlet operations produces another increase to the radial distortion. The significance of this increase in the radial distortion will need to be evaluated further.

D. Effect of a VG vane and a Hybrid vane/air jet configuration on distortion reduction and pressure recovery

The variation of the inlet circumferential distortion with changing inlet mass flow ratio for both the baseline (no flow control) and VG vane configurations are shown in figure 16. Both of these configurations are pictured in figure 17 and figure 18 showing the vane layout more clearly. Vane design details are shown in figure 10b[38]. In figure 16, the distortion trends with the inlet mass flow ratio show that the vane configuration was effective in reducing the inlet distortion level for almost the entire range of inlet mass flow settings. The baseline configuration distortion levels increases with inlet mass flow rate to go beyond the maximum target distortion level above an inlet mass flow ratio of about 0.38. The vane configuration was designed for an inlet mass flow ratio of 0.59. The AIP pressure contour in the lower right-hand portion of the figure demonstrates how effective the VG vanes are at evenly redistributing the boundary layer flow around the circumference of the diffuser exit, especially when compared to the baseline AIP pressure contour plot just above it.

For the vane configuration distortion, reducing the inlet mass flow rate below the design point caused the distortion to increase because of the reduced effectiveness of the vanes. Preliminary CFD simulations[37] of the vane configuration over this range of inlet mass flow rates have provided some reasons why the VG vane effectiveness decreases. These simulations show increased inlet flow spillage as the inlet mass flow rate is decreased, which is closely coupled with the increase in the size of two juncture vortices that reduce the velocity of the flow approaching the VG vanes.

The variation of the inlet pressure recovery with changing inlet mass flow rates for both the baseline and vane configurations is shown in figure 17. The baseline pressure recovery increases as the inlet mass flow rate increases

while that for the VG vane configurations does not change. Notice that the pressure recovery reductions between the baseline and vane configurations are consistent with the reductions observed for the control jet configurations. It is believed that installation issues for the vanes on a highly curved surface produced an aft facing step causing a downstream flow separation that may increase with an increase in the inlet mass flow rate. This is why the baseline pressure recovery is increasing with inlet mass flow rate increase while that for the vane configuration stays relatively constant.

Finally, the VG vane configuration produced unacceptable distortion levels for inlet mass flow rates (see figure 16) between about 0.44 and 0.47. To address this problem, a configuration was tested that added four control jets to work a short distance downstream of the vanes. An inset picture of the hybrid VG vane/jet control configuration is presented on the left side of figure 18. The reason for combining these two types of flow control devices was to balance the strengths and weaknesses of each device. The control jets require a significant amount of mass flow rate to effectively reduce the inlet distortion, but do not depend on the velocity of the onset flow to create a flow deflection force. The vanes do not require any external supply of mass flow rate to effectively reduce the inlet distortion, but do depend on the onset flow velocity to create a flow deflection force. Together, the vanes can reduce most of the inlet distortion and the control jets can be used at a significantly reduced control jet mass flow rate to make sure the inlet distortion stays low as the inlet mass flow rate varies. The hybrid configuration was tested at inlet mass flow rates where the distortion level was elevated. The addition of the four control jets to reduce the inlet distortion effectively kept the distortion level down to about 0.012 as the inlet mass flow decreased from 0.53. This was accomplished using a jet mass flow rate of about 0.4%.

IV. Conclusion

The goal of this research was to determine whether or not active flow control could be used to control the distortion levels for an S-inlet diffuser with significant BLI (35%). A systematic approach developed an actuator system with control jets configured to manage the inlet flow field. The flow control system had to manage two basic flow mechanisms inside the S-shaped inlet, the secondary flow and the significant BLI. There is a large body of research that deals with flow control handling the secondary flow at transonic Mach conditions. The study described in this paper is unique because it is the first known research to deal with both of these mechanisms at transonic Mach numbers over a range of inlet operating conditions. The high Mach number BLI inlet testing

provided a small-scale demonstration of the ability of an active flow control system to reduce the inlet flow distortion (circumferential). Although the flow control system developed is not optimal, insights were gained that can guide future research. The investigation included different control jet configurations, a VG vane configuration, and a hybrid or combination. During the investigation, the following was learned:

- For M=0.85, the application of active flow control steady jets operating at 1.5% of inlet mass flow for one jet distribution reduced the distortion from a $DPCP_{avg}$ value of 0.055 for the baseline to 0.025 for the active flow control case. This 16-jet configuration did not provide the lowest distortion level, but did prove to be the most effective by significantly reducing the distortion with the least amount of control jet mass flow rate. The minimum mass flow rate needed to meet the distortion goal of $DPCP_{avg} = 0.02$ was about 2.3% of the inlet mass flow. Increasing the control jets to 2.5% of the inlet mass flow for the 30-jet configuration continued to reduce the distortion to about 0.015. This configuration was considered the most effective at generating the lowest distortion levels.
- Balancing both the control jet momentum as well as the jet distribution is important in reducing inlet circumferential distortion. It is important to maximize the jet efficiency by selecting an optimal number of jets, producing the highest total jet momentum for a given jet mass flow rate, while also optimizing the spatial distribution of the selected jets.
- The measured pressure recovery decreases with significant BLI inlet flow control. This primarily occurs because of the viscous flow losses produced by the flow control methods. This flow control characteristic occurs for both the control jet and the VG vane configurations. It is conjectured that decreasing the 90° jet skew angle, which may have resulted in local flow separation near the jets, could reduce these losses. For the vane configuration, installation issues on a highly curved surface produced an aft-facing step potentially causing some downstream flow separation and the loss of some pressure recovery.
- The hybrid system that combined both VG vanes and control jets worked to keep the inlet distortion level low across the range of inlet mass flow rate settings requiring less than 0.5% of the inlet mass flow. The use of both devices emphasized the strengths of each device to maintain a given distortion level with a smaller jet mass-flow rate requirement.

Acknowledgments

This research was supported by the NASA Ultra Efficient Engine Technology (UEET) Highly Integrated Inlet (HII) project. Special thanks goes to Mr. Bobby Berrier for his guidance in the area of testing flush-mounted inlets. The authors would also like to acknowledge Mr. Tony Washburn and Ms. Judi Hannon for the significant contributions to the data acquisition hardware and software. Finally, special thanks to the entire NASA 0.3-meter TCT staff that helped make the experiment a successful one, especially Ms. Stacy Sigmon.

References

[1]Johnson, T., "Aviation's Environmental Impact on the Global Atmosphere," Proceedings of Aviation and the Environment – Their Future in an Integrated Transport Policy, RAE, London, 1999, pp. 13.1-13.5.

[2]Green, J. E., "Air Travel- Greener by Design, Mitigating the environmental impact of aviation: Opportunities and priorities," *The Aeronautical Journal of the Royal Aeronautical Society*, v 109, no 1099, September 2005, pp. 361-416.

[3]Brown, A. S., "HSR Work Propels UEET Program (High Speed Research in Ultra-efficient Engine Technology in Aircraft Industry)," *Aerospace America*, Vol. 37, No. 5, May 1999, pp. 48-50.

[4]Callaghan, J. T., and Liebeck, R. H., "Some Thoughts on the Design of Subsonic Transport Aircraft for the 21st Century," Cockpit, Dec. 1990, pp. 5-13.

[5]Liebeck, R. H., Page, M. A., Rawdon, B. K., "Evolution of the Revolutionary Blended-Wing-Body," Transportation Beyond 2000: Technologies Needed for Engineering Design," February, 1996, pp. 431-459.

[6]Liebeck, R. H.,"Design of the Blended-Wing-Body Subsonic Transport," AIAA 2002-002.

[7]Daggett, D. L., "Ultra Efficient Engine Technology Systems Integration and Environmental Assessment," NASA CR-2002-211754, July 2002.

[8]Anabtawi, A. J., Blackwelder, R. F., Lissaman, P. B. S., Liebeck, R. H., "An Experimental Investigation of Boundary Layer Ingestion in a Diffusing S-Duct With and Without Passive Flow Control," AIAA 99-0739.

[9]Anderson, B. H., and Gibb, J., "Vortex Generator Installation Studies on Steady State and Dynamic Distortion," AIAA 96-3279, July, 1996.

[10]Lin, J. C., "Review of Research on Low-Profile Vortex Generators to Control Boundary-Layer Separation," *Progress in Aerospace Sciences*, Vol 38, p 389-420, 2002.

[11]Anderson, B. H., Baust, H. D., and Agrell, J., "Management of Total Pressure Recovery, Distortion and High Cycle Fatigue in Compact Air Vehicle Inlets," NASA TM-2002-212000, December, 2002.

[12]Anderson, B. H., Miller, D. N., Yagle, P. J., and Truax, P. P., "A Study on MEMS Flow Control For the Management of Engine Face Distortion in Compact Inlet Systems," Proceedings of the 3rd ASME/JSME Joint Fluids Engineering Conference, July, 1999.

[13]Hamstra, J. W., Miller, D. N., Truax, P. P., Anderson, B. H., and Wendt, B. J., "Active Inlet Flow Control Technology Demonstration," *The Aeronautical Journal of the Royal Aeronautical Society*, October, 2000.

[14]Seddon, J., and Goldsmith, E. L., *Intake Aerodynamics*, Second Edition, AIAA, Reston, Virginia, 1999, p. 169, 278-285.

[15]Gorton, S. A., Owens, L. R., Jenkins, L. N., Allan, B. G., and Schuster, E. P., "Active Flow Control on a Boundary-Layer-Ingesting Inlet, " AIAA-2004-1203.

[16]Lord, W. K., MacMartin, D. G., and Tillman, T. G., "Flow Control Opportunities in Gas Turbine Engines," AIAA 2000-2234.

[17]Vakili, A. D., Wu, J. M., Liver, P., and Bhat, M. K., "Flow Control in a Diffusing S-Duct," AIAA 85-0524.

[18]Smith, B. L., and Glezer, A., "The Formation and Evolution of Synthetic Jets," *Physics of Fluids*, Vol. 10, No. 9, 1998.

[19]Barberopoulos, A. A., and Garry, K. P., "The Effect of Skewing on the Vorticity Produced by an Airjet Vortex Generator," *The Aeronautical Journal of the Royal Aeronautical Society*, v 102, no 1013, March 1998, pp. 171-179.

[20]Tilmann, C. P., Langan, K. J., Betterton, J. G., and Wilson, M. J., "Characterization of Pulsed Vortex Generator Jets for Active Flow Control," Presented at the RTO AVT Symposium on Active Control Technology for Enhanced Performance Operation Capabilities of Military Aircraft, Land Vehicles and Sea Vehicles, Germany, May, 2000.

[21]Peake, D. J., Henry, F. S., and Pearcey, H. H., "Viscous Flow Control with Air-Jet Vortex Generators," AIAA 99-3175, June, 1999.

[22]Crook, A., and Wood, N. J., "Measurements and Visualizations of Synthetic Jets," AIAA 2001-0145.

[23]Wygnanski, I., "Some New Observations Affecting the Control of Separation by Periodic Excitation," AIAA 2000-2314, June, 2000.

[24]Washburn, A. E., Gorton, S. A., and Anders, S. G., "Snapshot of Active Flow Control Research at NASA Langley," AIAA 2002-3155.

[25]Schaeffler, N. W., Hepner, T. E., Jones, G. S., and Kegerise, M. A., "Overview of Active Flow Control Actuator Development at NASA Langley Research Center," AIAA 2002-3159.

[26]Sellers, W. L., III, Jones, G. S., and Moore, M. D., "Flow Control Research at NASA Langley in Support of High-Lift Augmentation," AIAA 2002-606.

[27]Rao, N. M., Feng, J., Burdisso, R. A., and Ng, W. F., "Experimental Demonstration of Active Flow Control to Reduce Unsteady Stator-Rotor Interaction," *AIAA Journal*, v 39, no 3, March 2001, p 458-464.

[28]Jenkins, L. N., Gorton, S. A., and Anders, S. G., "Flow Control Device Evaluation for an Internal Flow with an Adverse Pressure Gradient," AIAA 2002-0266.

[29]Berrier, B. L., "Evaluation of Flush-Mounted, S-Duct Inlets with Large Amounts of Boundary Layer Ingestion," RTO Vehicle Propulsion Integration Symposium, Warsaw, Poland, October, 2003.

[30]Berrier, B. L., and Allan, B. G., "Experimental and Computational Evaluation of Flush-Mounted, S-Duct Inlets (Invited), " AIAA-2004-0764.

[31]Berrier, B. L., Carter, M. B., and Allan, B. G., "High Reynolds Number Investigation of a Flush-Mounted, S-Duct Inlet with Large Amounts of Boundary Layer Ingestion, " NASA TP-2005-213766, September 2005.

[32]Allan, B. G., Owens, L. R., and Berrier, B. L., "Numerical Modeling of Active Flow Control in a Boundary Layer Ingesting Offset Inlet, " AIAA-2004-2318.

[33]Mineck, R. E., and Hill, A. S., "Calibration of the 13- by 13-Inch Adaptive Wall Test Section for the Langley 0.3-Meter Transonic Cryogenic Tunnel, " NASA TP-3049, December 1990.

[34]Rallo, R. A., Dress, D. A., and Siegle, H. J. A., "Operating Envelope Charts for the Langley 0.3-Meter Transonic Cryogenic Wind Tunnel, " NASA TM-89008, August 1986.

[35]*Gas Turbine Engine Inlet Flow Distortion Guidelines*. Aerospace Recommended Practice 1420B, SAE International, 2001.

[36]*Instruments and Apparatus*. "Part I – Measurement Uncertainty," ANSI/ASME PTC 19.1-1985, American National Standards Inst., 1985.

[37]Allan, B. G., and Owens, L. R., "Numerical Modeling of Flow Control in a Boundary-Layer-Ingesting Offset Inlet Diffuser at Transonic Mach Numbers, " AIAA-2006-0845.

[38]Allan, B. G., Owens, L. R., and Lin, J. C., "Optimal Design of Passive Flow Control for a Boundary-Layer-Ingesting Offset Inlet Using Design-of-Experiments, " AIAA-2006-1049.

Tables

Table 1. Inlet characteristics

Average wall angle (ϕ) [deg]	18.3
Inlet length (L) [in.]	7.696
Inlet offset height (ΔH) [in.]	2.543
Exit diameter (D_2) [in.]	2.448
Inlet throat area (A_i) [sq. in.]	4.400
Inlet capture (highlight) area (A_C) [sq. in.]	5.760
Diffuser exit area (A_2) [sq. in.]	4.704
Inlet throat height (H_i) [in.]	1.703
Inlet throat width (W_i) [in.]	3.249
Inlet lip length (a) [in.]	0.479
Inlet lip height (b) [in.]	0.240
Cowl forebody length (X) [in.]	0.713
Cowl maximum height (H_{max}) [in.]	2.185
Cowl aftbody length (X_{aft}) [in.]	14.610
Cowl aftbody boattail angle [deg]	11.0
Design throat Mach number	0.70

Table 3. Uncertainty estimates

Parameter	Uncertainty
M	±0.003
P_t	±0.1 psia
T_t	±0.2°F
U/U_e	±0.01
$P_{t,2}$	±0.06 psia
Spatial distances	±0.005 inches
Distortion	±0.001
Pressure Recovery	±0.004
Inlet mass flow	±0.02 lbm/s
Control Jet mass flow	±0.002 lbm/s or ±0.1% of Inlet Mass Flow Rate as plotted (referenced to an inlet mass flow rate of 2 lbm/s)
A_0/A_C	±0.006

Table 2. Predicted BWB full/model-scale corrected inlet airflow values

Altitude, ft	Mach	Condition	Net Thrust, lbf	Full-scale Corrected Airflow, lbm/s	2.5%-scale Corrected Airflow, lbm/s	A_O/A_C	
36089	0.85	Max Climb	14555	2081	1.30	0.65	
		Max Cruise	13976	2062	1.29	0.64	
		Part Power	13277	2038	1.27	0.63	
			12590	2012	1.26	0.62	
			11180	1950	1.22	0.60	
			9784	1882	1.18	0.58	
			8384	1811	1.13	0.56	
			6989	1737	1.09	0.54	
			5591	1659	1.04	0.51	Testing Range Overlap
			4193	1559	0.97	0.48	
			2793	1468	0.92	0.46	

Captions

Figure 1. A version of the Blended-Wing-Body configuration is shown.

Figure 2. The effect of BLI on range increase as a function of bypass ratio (BPR).

Figure 3. The BLI inlet design parameters shown on a side-view sketch of model centerline.

Figure 4. BLI inlet model as installed in the 0.3-meter TCT test section.

Figure 5. Boundary layer profiles obtained in the BLI Inlet investigation.

Figure 6. Asymmetric effect of boundary layer rake installation on the measured AIP total pressures.

Figure 7. Bottom view of inlet model showing the final adaptive wall positions used throughout the flow control experiment.

Figure 8. Local Mach distribution from tunnel wall centerline pressure measurements at M=0.88, P_t=30 psia, T_t=80°F, A_0/A_C=0.54.

Figure 9. A view of the left (looking upstream) half of the inlet diffuser is shown to illustrate all available jet locations and the general location of the vortex generators when installed.

Figure 10. Some details about the flow control layout used in this investigation.

Figure 11. Effects of tunnel total pressure variation (Re_D) on distortion reduction in BLI inlet experiment for M=0.85, T_t=80ºF, A_0/A_C=0.54, configuration 10 with 36 jets.

Figure 12. Effects of tunnel total pressure variation (Re_D) on pressure recovery with AFC in BLI inlet test for M=0.85, T_t=80ºF, A_0/A_C=0.54, configuration 10 with 36 jets.

Figure 13. Control jet momentum and distribution effect on circumferential distortion reduction in BLI inlet experiment for M=0.85, P_t=30 psia, T_t=80ºF, A_0/A_C=0.54.

Figure 14. Control jet momentum and distribution effect on pressure recovery in BLI inlet experiment for M=0.85, P_t=30 psia, T_t=80ºF, A_0/A_C=0.54.

Figure 15. Typical radial distortion character as control jets reduce circumferential distortion in BLI inlet test for M=0.85, P_t=30 psia, T_t=80ºF, A_0/A_C=0.54.

Figure 16. VG vane control effect on distortion reduction in BLI inlet experiment for M=0.85, P_t=30 psia, T_t=80ºF.

Figure 17. VG vane control effect on pressure recovery in BLI inlet experiment for M=0.85, P_t=30 psia, T_t=80ºF.

Figure 18. Combined vane and jet control effect on distortion reduction in BLI inlet test for M=0.85, P_t=30 psia, T_t=80ºF, configuration 11 VGs with four jets.

Figures

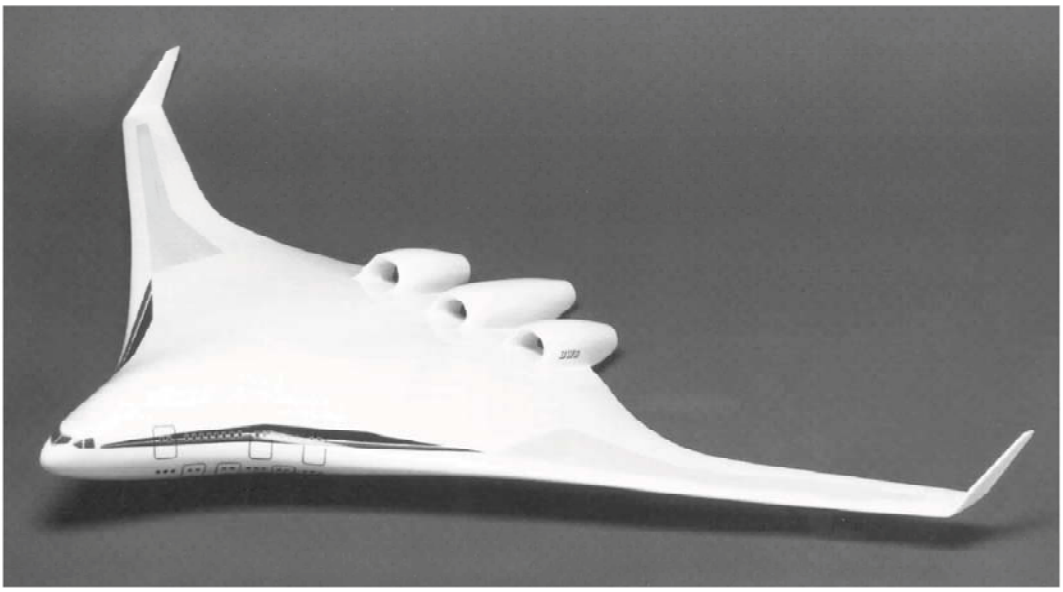

Figure 1. A version of the Blended-Wing-Body configuration is shown.

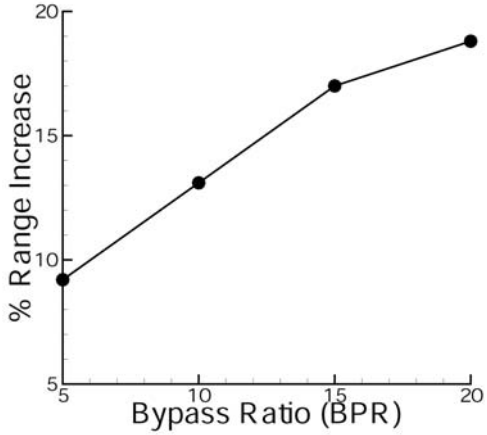

Figure 2. The Effect of BLI on range increase as a function of bypass ratio (BPR).

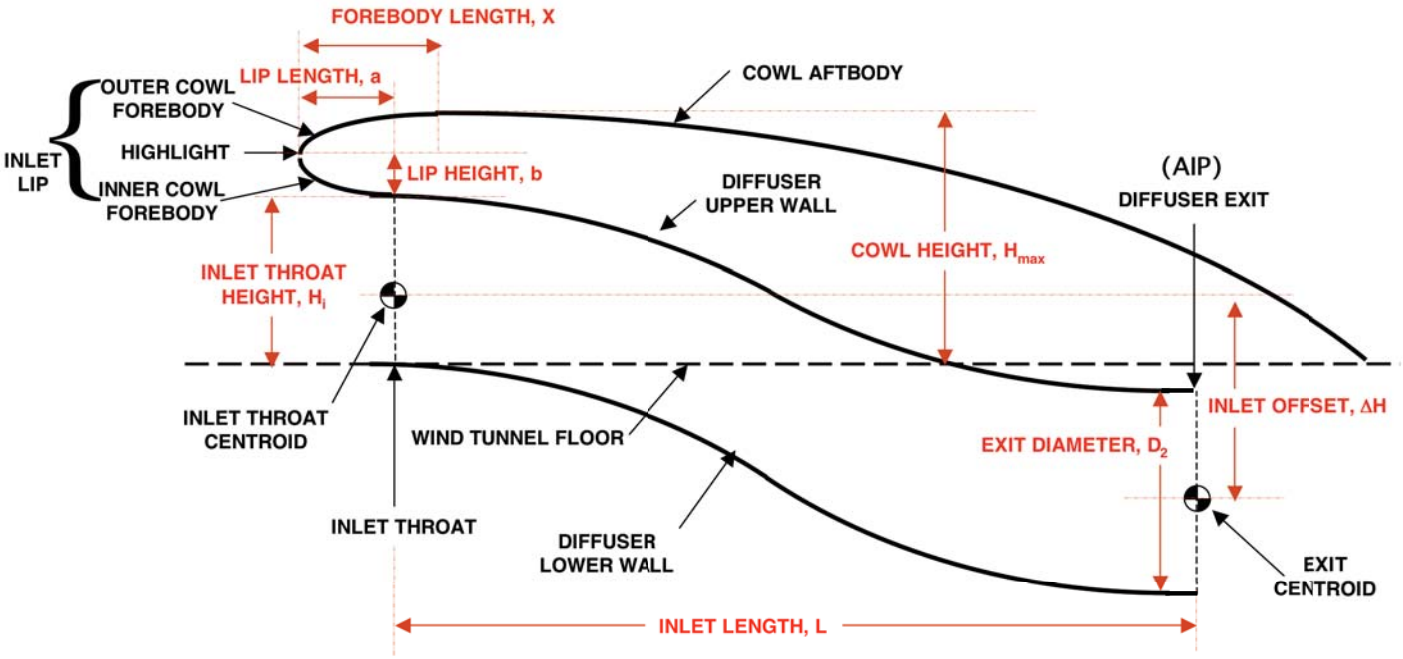

Figure 3. The BLI inlet design parameters shown on a side-view sketch of model centerline.

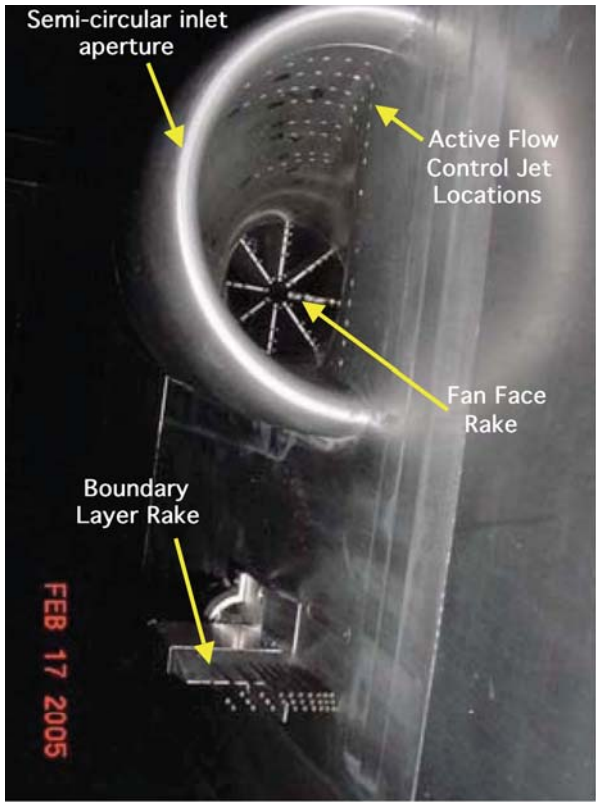

a) Inlet model front view

Figure 4. BLI inlet model as installed in the 0.3-meter TCT test section.

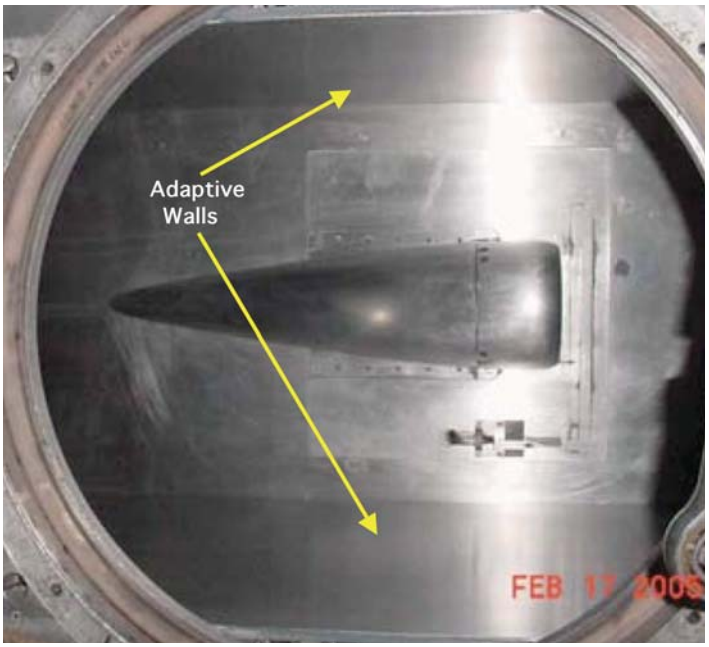

b) Inlet model top view

Figure 4. Concluded.

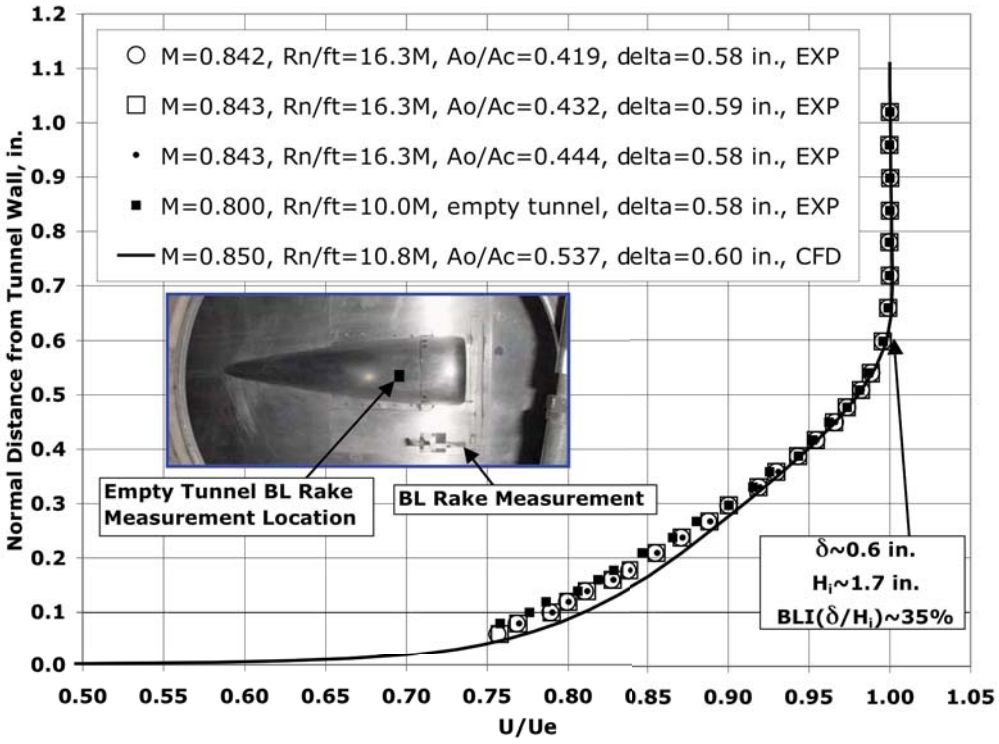

Figure 5. Boundary layer profiles obtained in the BLI inlet investigation.

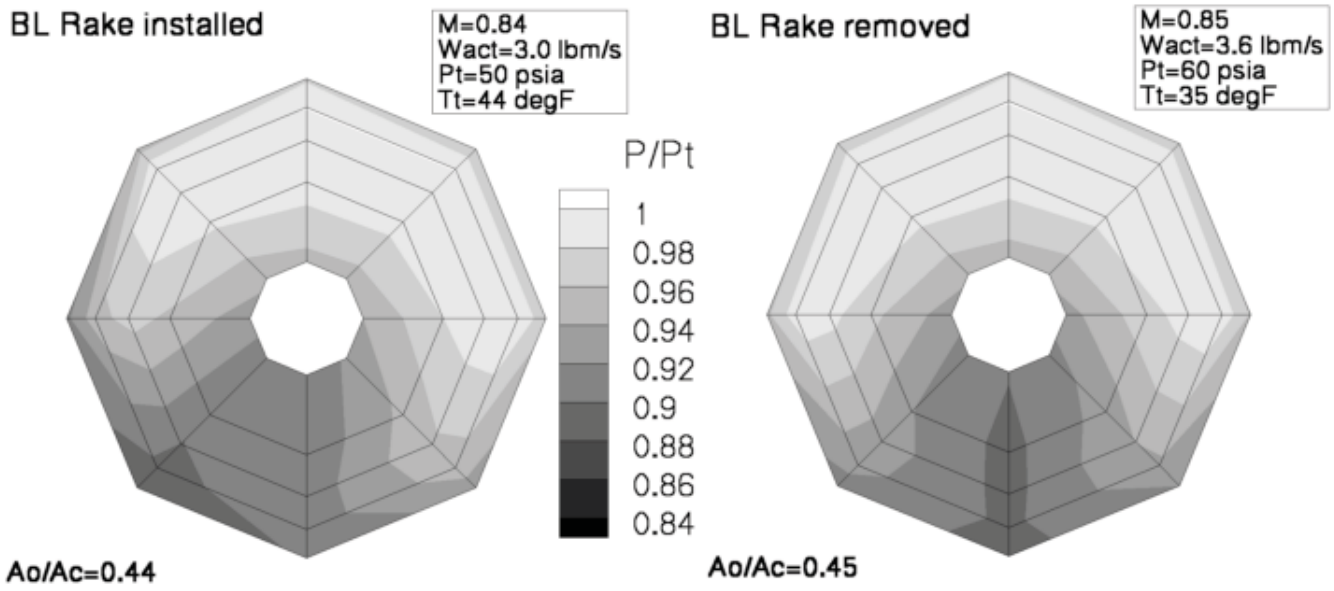

Figure 6. Asymmetric effect of boundary layer rake installation on the measured AIP total pressures.

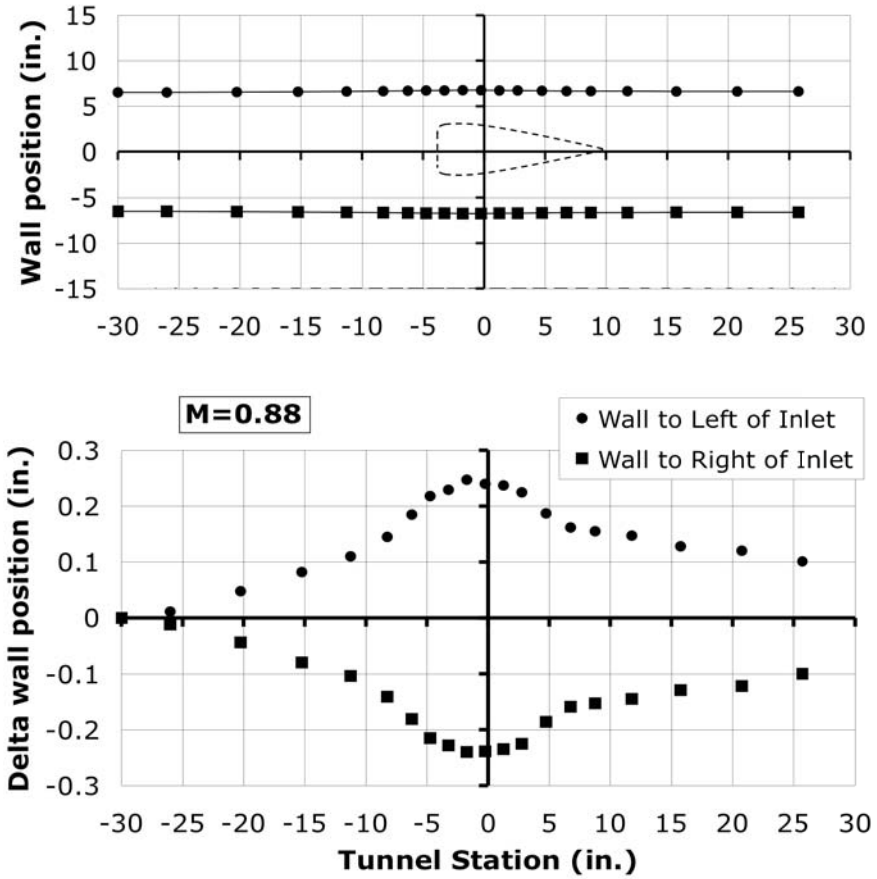

Figure 7. Bottom view of inlet model showing the final adaptive wall positions used throughout the flow control experiment.

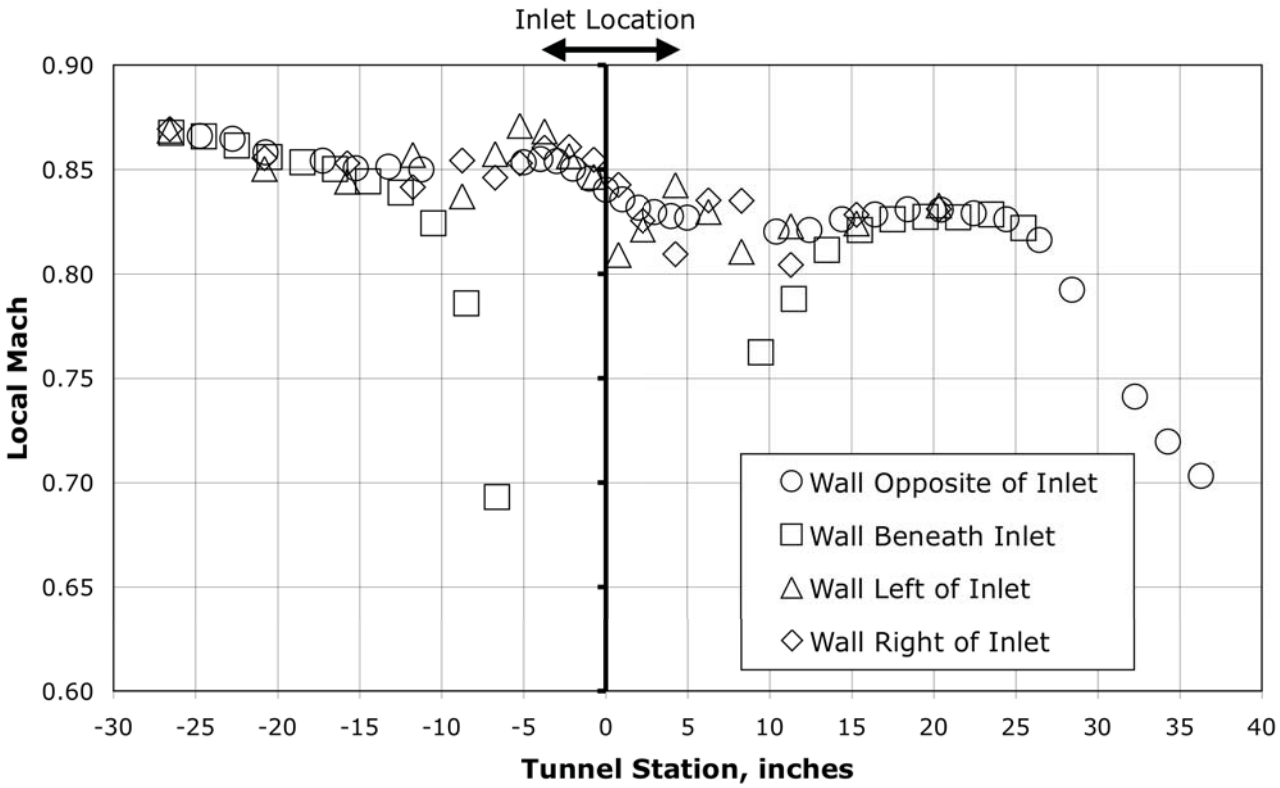

Figure 8. Local Mach distribution from tunnel wall centerline pressure measurements at M=0.88, P_t=30 psia, T_t=80°F, A_0/A_C=0.54.

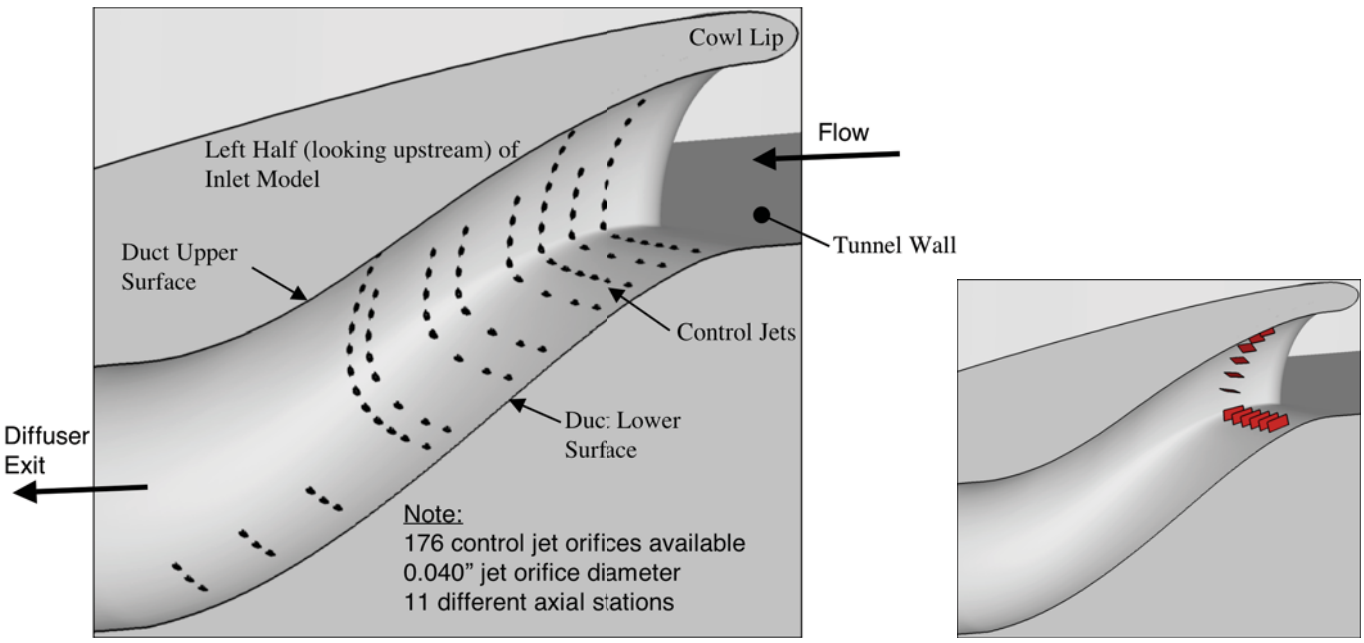

Figure 9. A view of the left (looking upstream) half of the inlet diffuser is shown to illustrate all available jet locations and the general location of the vortex generators when installed.

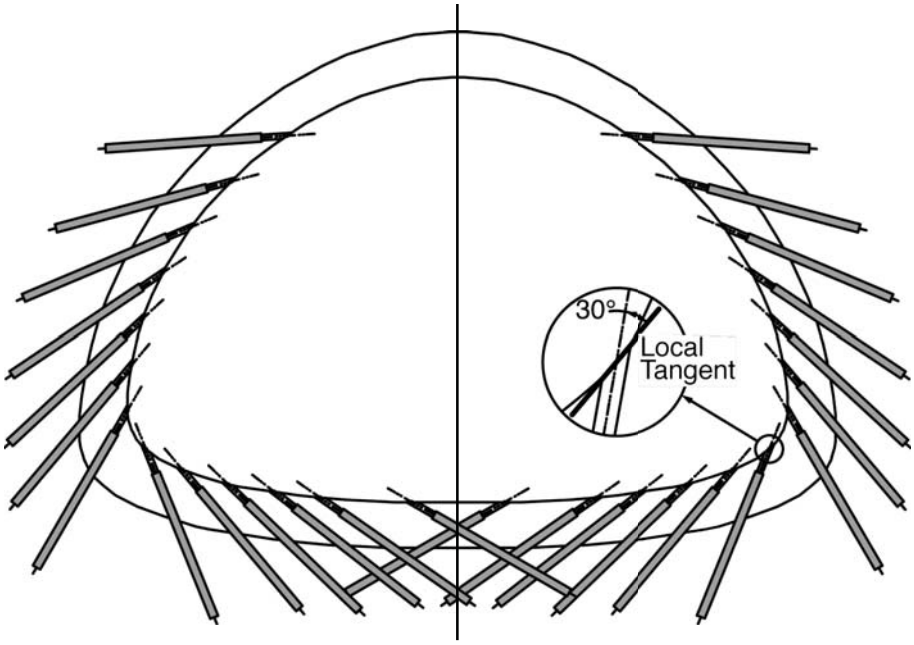

a) Control jets orientation within a vertical plane at each axial station.

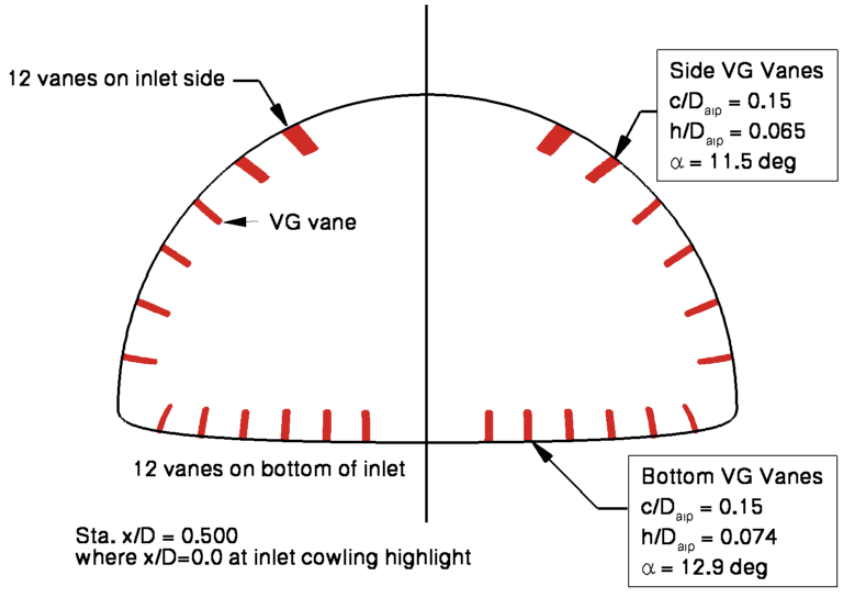

b) VG vane layout in the diffuser

Figure 10. Some details about the flow control layout used in this investigation.

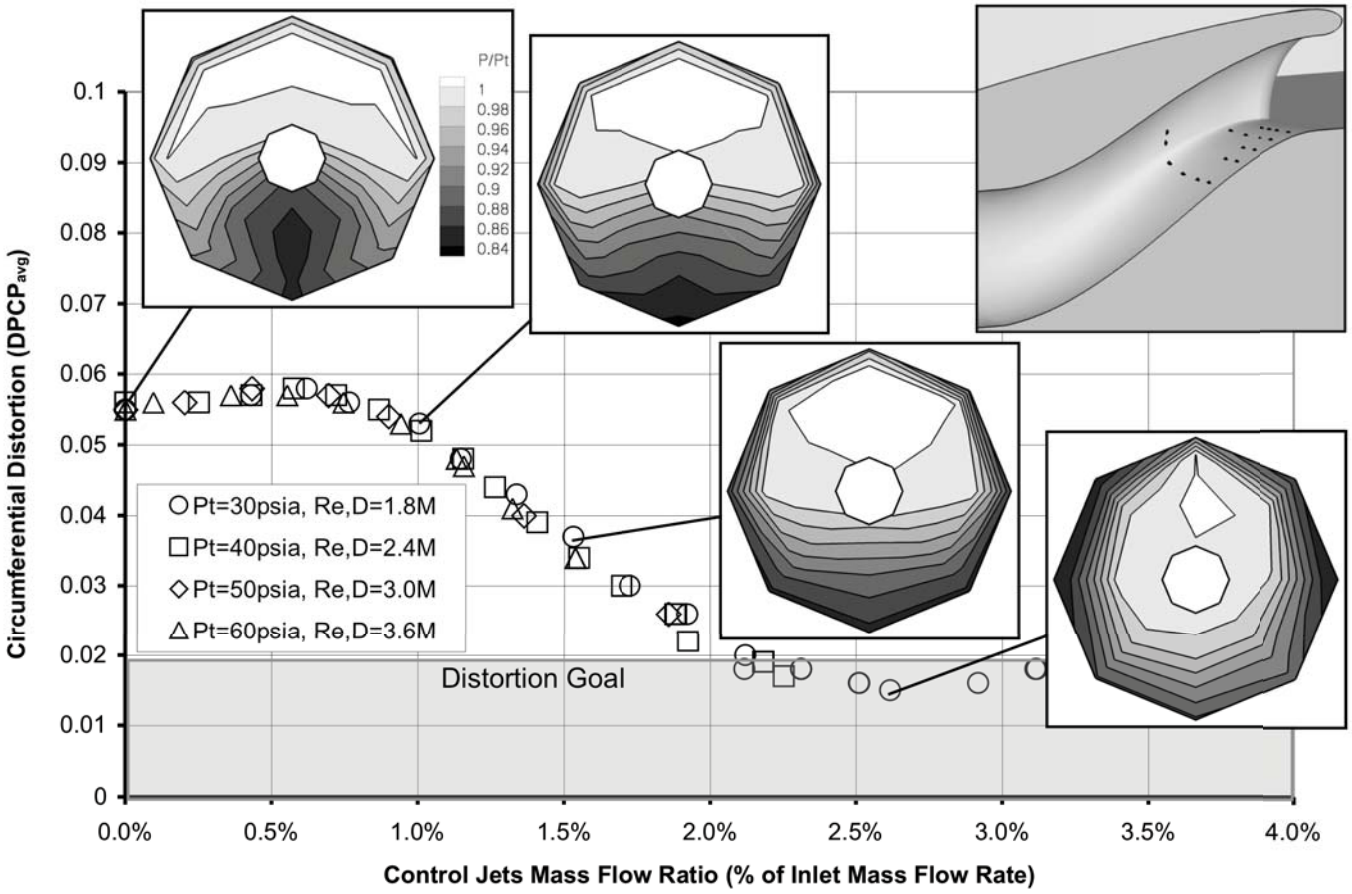

Figure 11. Effects of tunnel total pressure variation (Re_D) on distortion reduction in BLI inlet experiment for M=0.85, T_t=80°F, A_0/A_C=0.54, configuration 10 with 36 jets.

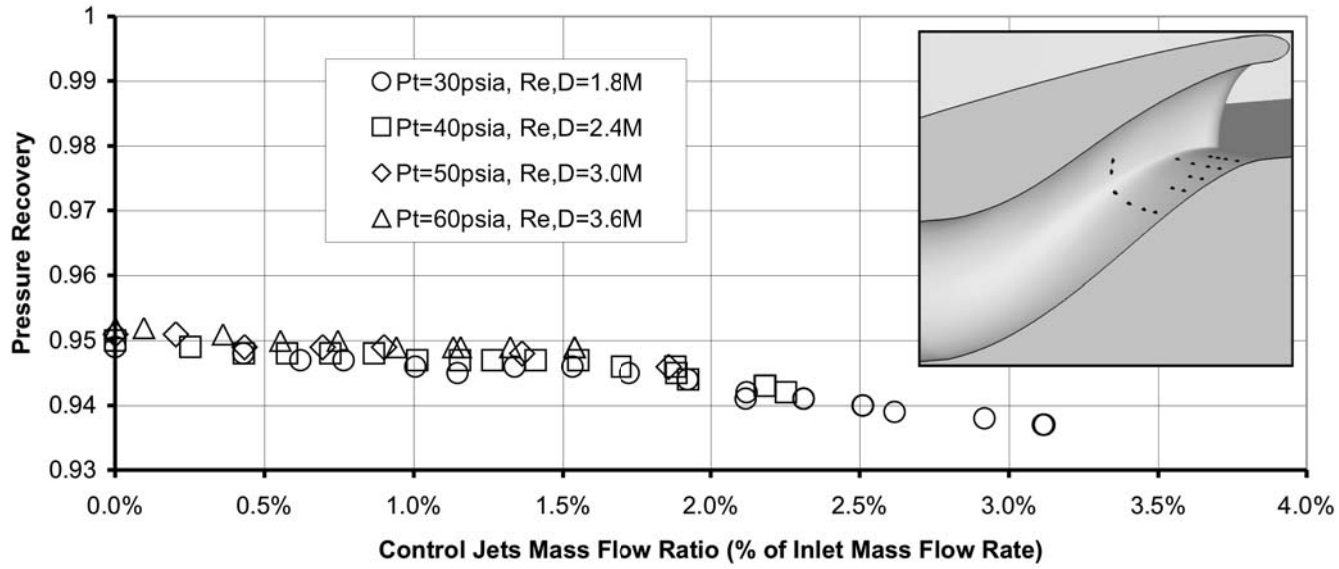

Figure 12. Effects of tunnel total pressure variation (Re_D) on pressure recovery with AFC in BLI inlet test for M=0.85, T_t=80°F, A_0/A_C=0.54, configuration 10 with 36 jets.

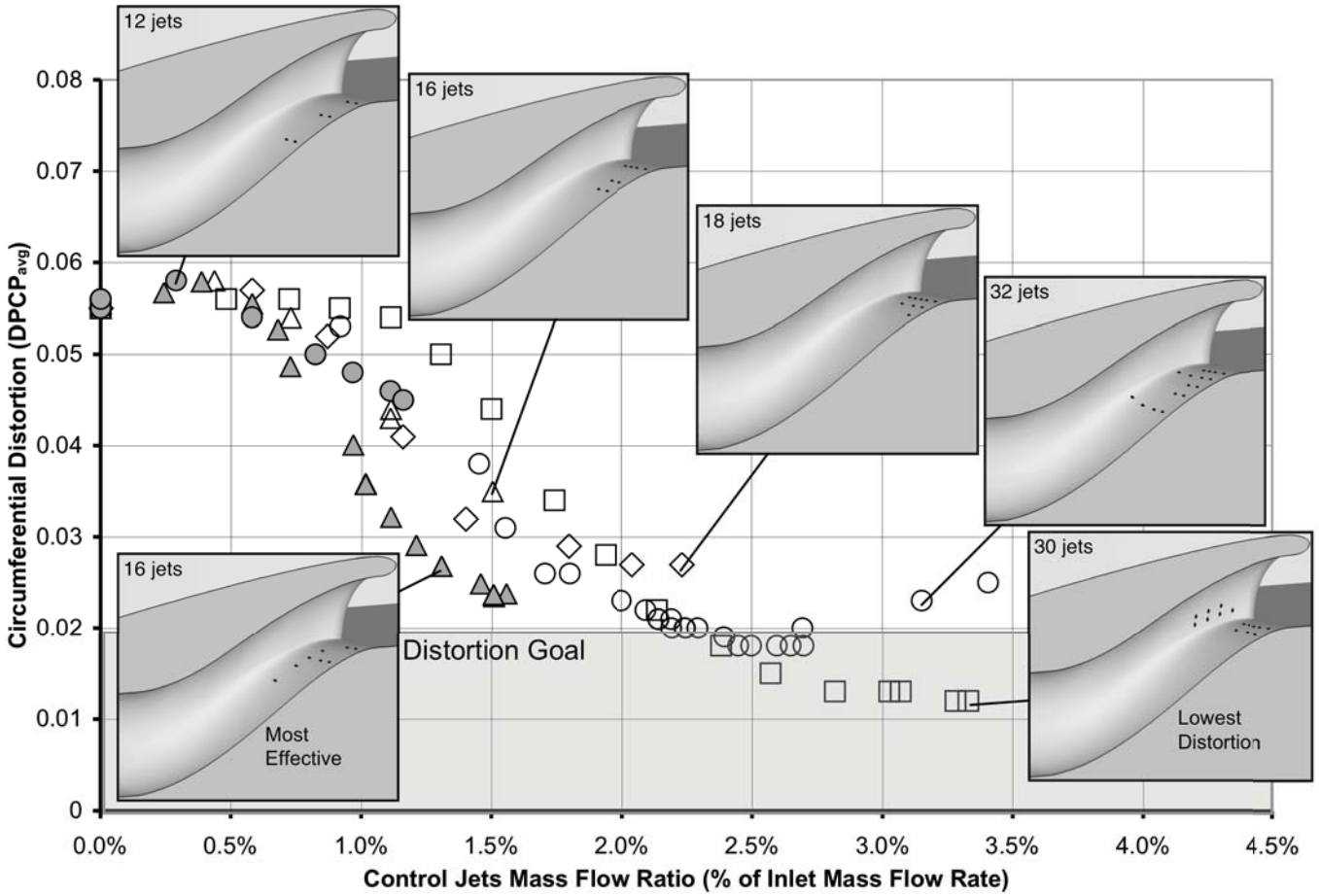

Figure 13. Control jet momentum and distribution effect on circumferential distortion reduction in BLI inlet experiment for M=0.85, P_t=30 psia, T_t=80°F, A_0/A_C=0.54.

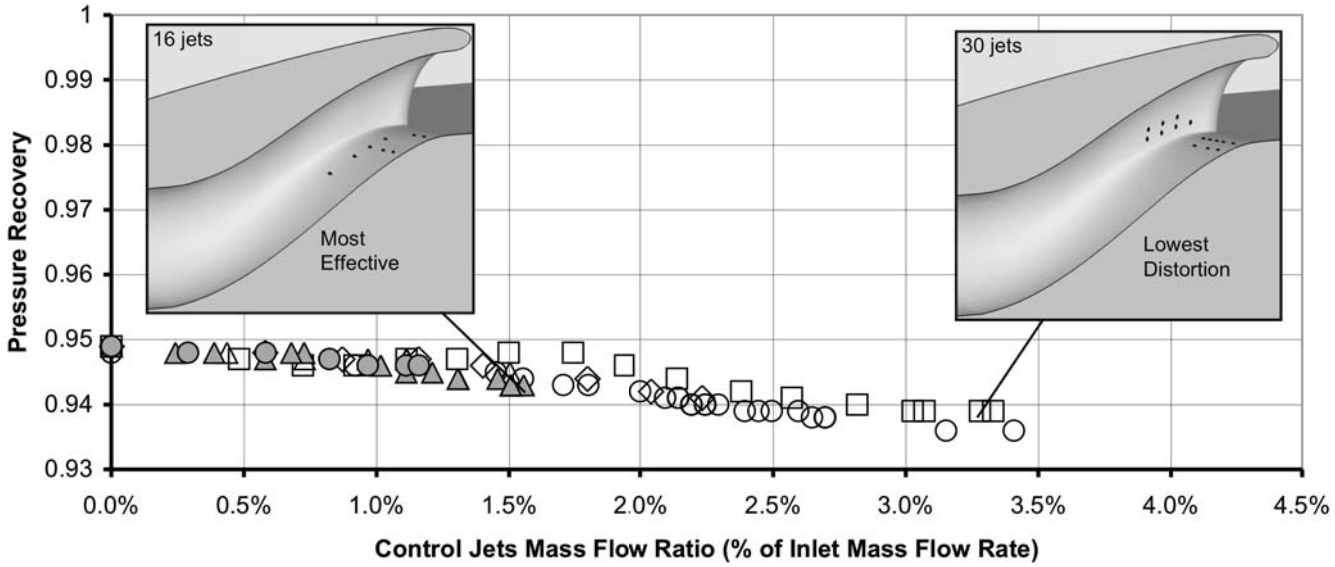

Figure 14. Control jet momentum and distribution effect on pressure recovery in BLI inlet experiment for M=0.85, P_t=30 psia, T_t=80°F, A_0/A_C=0.54.

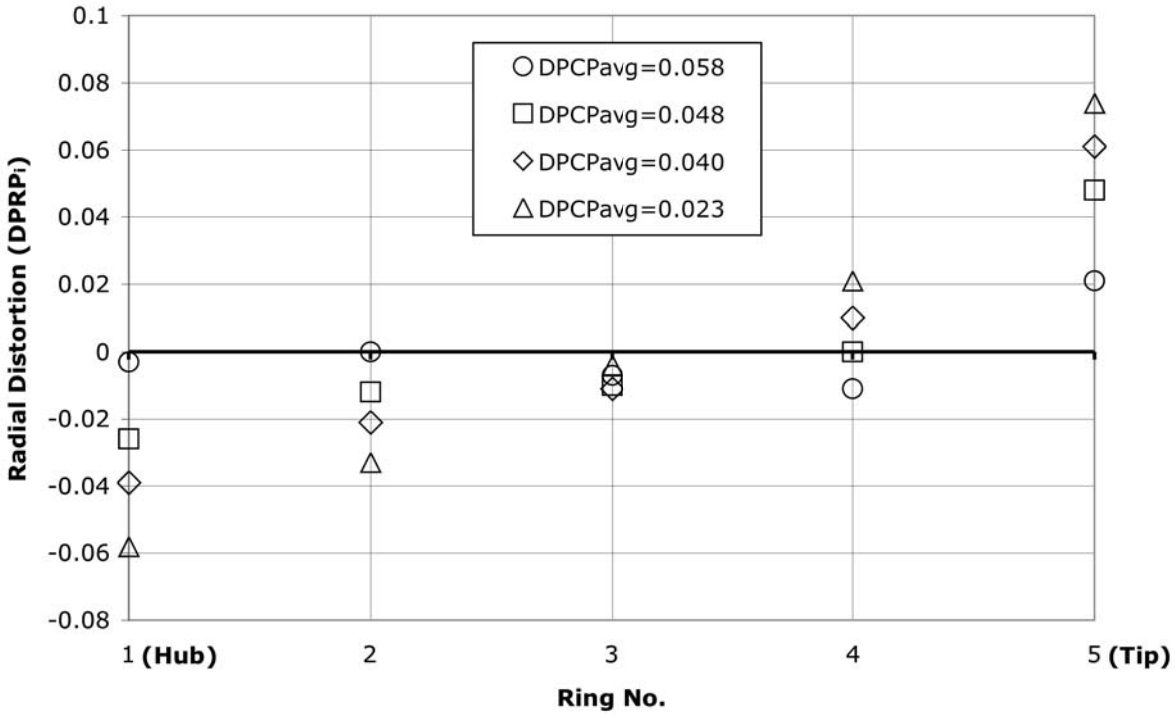

Figure 15. Typical radial distortion character as control jets reduce circumferential distortion in BLI inlet test for M=0.85, P_t=30 psia, T_t=80°F, A_0/A_C=0.54.

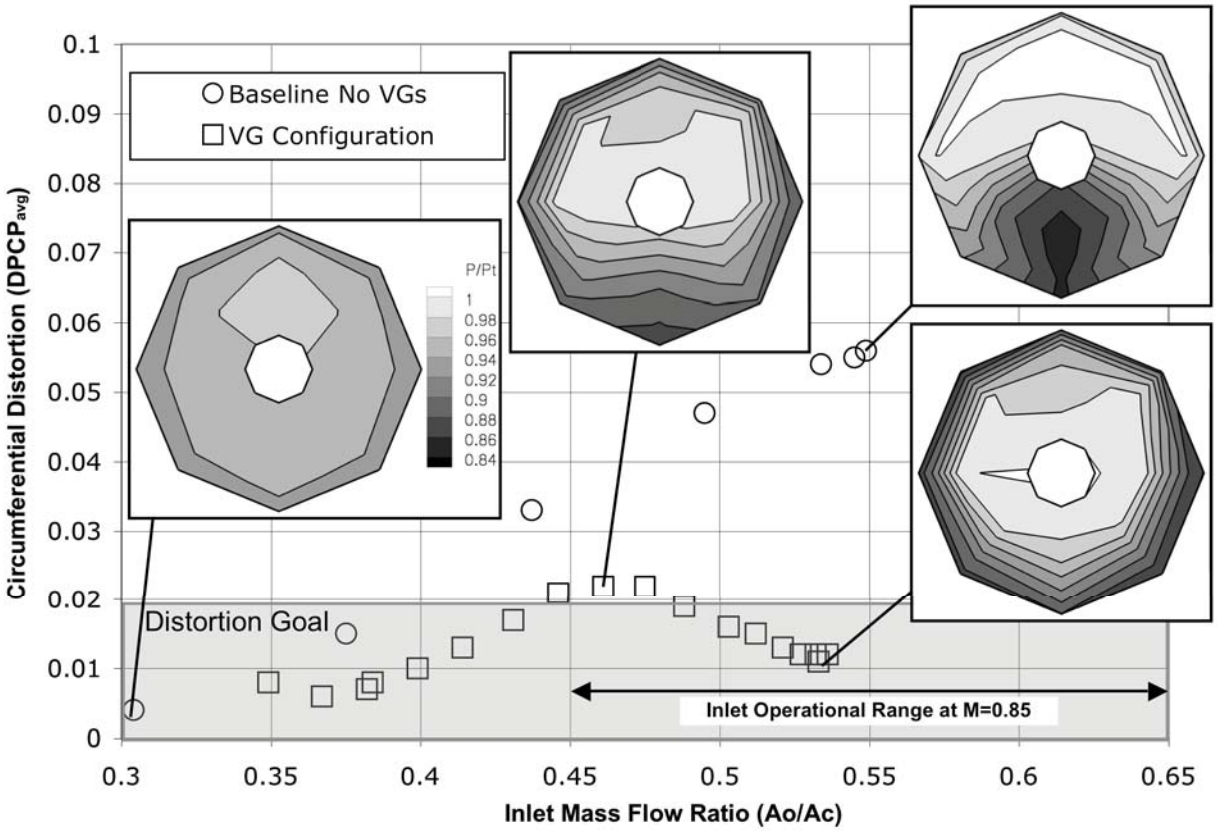

Figure 16. VG vane control effect on distortion reduction in BLI inlet experiment for M=0.85, P_t=30 psia, T_t=80°F.

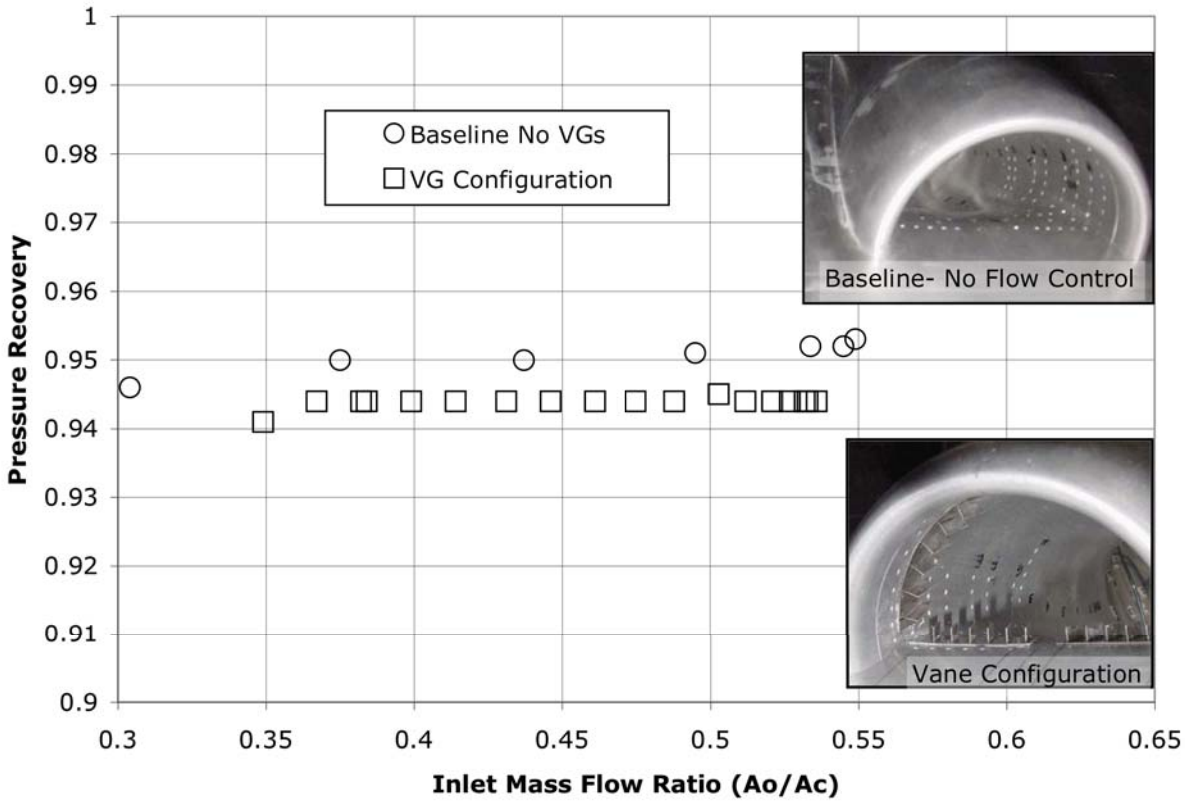

Figure 17. VG vane control effect on pressure recovery in BLI inlet experiment for M=0.85, P_t=30 psia, T_t=80°F.

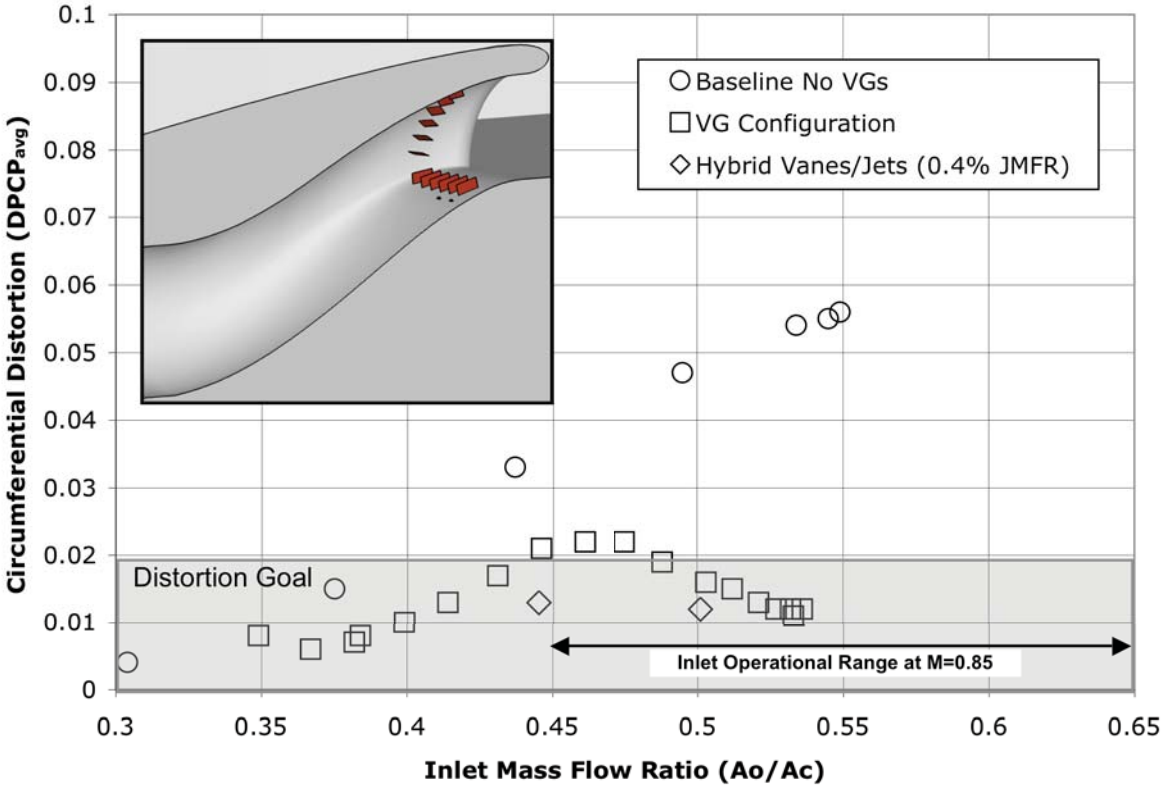

Figure 18. Combined vane and jet control effect on distortion reduction in BLI inlet test for M=0.85, P_t=30 psia, T_t=80°F, configuration 11 VGs with four jets.